Editors' Suggestion

Underlying Topological Dirac Nodal Line Mechanism of the Anomalously Large Electron-Phonon Coupling Strength on a Be (0001) Surface

Ronghan Li,[1,2,†] Jiangxu Li,[1,2,†] Lei Wang,[1,2] Jiaxi Liu,[1,2] Hui Ma,[1] Hai-Feng Song,[3] Dianzhong Li,[1,2] Yiyi Li,[1,2] and Xing-Qiu Chen[1,2,*]

[1]*Shenyang National Laboratory for Materials Science, Institute of Metal Research, Chinese Academy of Science, 110016 Shenyang, Liaoning, People's Republic of China*

[2]*School of Materials Science and Engineering, University of Science and Technology of China, Heifei 230026, People's Republic of China*

[3]*Institute of Applied Physics and Computational Mathematics, Beijing 100094, People's Republic of China*

(Received 20 December 2018; revised manuscript received 8 August 2019; published 23 September 2019)

Beryllium has recently been discovered to harbor a Dirac nodal line (DNL) in its bulk phase and the DNL-induced nontrivial surface states (DNSSs) on its (0001) surface, rationalizing several already-existing historic puzzles [Phys. Rev. Lett. **117**, 096401 (2016)]. However, to date the underlying mechanism as to why its (0001) surface exhibits an anomalously large electron-phonon coupling effect ($\lambda^s_{e\text{-ph}} \approx 1.0$) remains unresolved. Here, by means of first-principles calculations, we show that the coupling of the DNSSs with the phononic states mainly contributes to its novel surface e-ph enhancement. Besides the fact that the experimentally observed $\lambda^s_{e\text{-ph}}$ and the main Eliashberg coupling function (ECF) peaks are reproduced well in our current calculations, we decompose the ECF $\alpha^2F(k,\boldsymbol{q};v)$ and the e-ph coupling strength $\lambda(k,\boldsymbol{q};v)$ as a function of each electron momentum (k), each phonon momentum ($\boldsymbol{q}$), and each phonon mode (v), evidencing the robust connection between the DNSSs and both $\alpha^2F(k,\boldsymbol{q};v)$ and $\lambda(k,\boldsymbol{q};v)$. The results reveal the strong e-ph coupling between the DNSSs and the phonon modes, which contributes over 80% of the $\lambda^s_{e\text{-ph}}$ coefficient on the Be (0001) surface. It highlights that the anomalously large e-ph coefficient on the Be (0001) surface can be attributed to the presence of its DNL-induced DNSSs, clarifying the long-debated mechanism.

DOI: 10.1103/PhysRevLett.123.136802

The class of topological Dirac nodal line semimetals (DNLs) [1–59] exhibits fully closed lines around the Fermi level due to the continuously linear crossings of the bulk energy bands. If a DNL is enforced by the inversion (P) and time-reversal (T) symmetry without the spin-orbit coupling (SOC), in the region inside of the DNL in k-lattice momenta, the occupied bands exhibit a π Berry phase along the normal direction of the DNL. The projection of the DNLs onto a certain surface would result in a closed ring, in which the topologically protected DNL-induced nontrivial surface states (DNSSs) occur. Usually, the DNSSs are not strictly flat drumheadlike states, with some certain dispersions upon interaction energies and details of specified surfaces of real DNL materials [38,41]. Although topological protection of the drumhead surface states is not necessarily guaranteed, the bound surface charge per unit momentum squared is always present within the projected interior of the DNL, even in the strongly particle-hole broken limit [38,41,44] due to the quantized polarization in bulk states. These kinds of exotic band structures render various novel properties. In addition to the common DNSSs-induced high electronic density around the Fermi energy, there are still giant surface Friedel oscillations [5], flat Landau levels [58], long-range Coulomb interaction [59], special collective modes [23], flat optical conductivity [27–30], giant magnetoresistance and mobility [26], and an unconventional enhancement of effective mass [31], as well as a potential route to achieve high-temperature superconductivity [20–22] and catalytic candidates [49], and so on.

Recently, we have found that bulk Be metal, crystallizing in the hexagonal $P6_3/mmc$ space group, hosts the DNL at its $k_z = 0$ plane of the BZ surrounding the centered Γ point due to the band inversion between Be s- and p_z-like orbits [5]. The DNL in Be is protected by the PT symmetries with extremely weak SOC, leading to a topological nontrivial π Berry phase of the occupied bands in the region inside the DNL along its normal direction [38,41] and the zero monopole charge [39–41] (see Supplemental Material text I and Fig. S1 [60]). Using the weak spin-orbit coupling Fu-Kane topological invariant method [41], its Z_2 index has been analyzed to be (1;0,0,0). Interestingly, this DNL-induced DNSSs rationalize three already-existing historic puzzles [61–68] of (i) the surface states observed by the angle-resolved photoemission spectroscopy (ARPES) experiments, (ii) the severe deviations of its surface electronic structures from the description of the nearly free electron picture, and (iii) the giant Friedel oscillations. Although these three puzzles have been resolved, the origin of its anomalously large electron-phonon (e-ph) coupling strength on the (0001) surface still remains open.

As early as 1998, the e-ph coupling strength on the Be (0001) surface $\lambda^s_{e\text{-ph}}$ was measured to be 1.15 ± 0.1 or 1.18 ± 0.07 by the ARPES experiment [69,70], being about 5 times the bulk Be value $\lambda^b_{e-\text{ph}} = 0.24$ [71,72]. On the basis of these measurements, the surface superconductivity was suggested to exist [69]. Subsequent ARPES experiments reported that the $\lambda^s_{e\text{-ph}}$ was in the range from 0.6 to 1.18 [69,70,73–77], mainly because of the anisotropic e-ph interaction on the Be (0001) $\bar{\Gamma}$ surface states [78]. Furthermore, the reported low $\lambda^s_{e-\text{ph}} = 0.6$ [73] was experimentally caused by surface oxygen contamination [78]. The known *ab initio* calculations for the e-ph coupling on the Be (0001) surface did not reproduce the measurements [78,79]. The early density-functional theory (DFT)-derived $\lambda^s_{e\text{-ph}}$ was 0.90 [75,80], which was thought to be wrong [78] due to a programming error. The latest ARPES experiments [79] even claimed that none of the main experimental Eliashberg coupling function (ECF) peaks in the low-frequency range was captured by the previous calculations [75,80]. Therefore, these discrepancies between experimental and theoretical findings would also need to be urgently clarified.

Returning to the fact that bulk Be exhibits the DNL and the DNL-induced DNSSs on its (0001) surface [5], we have strongly suspected whether or not the DNSSs result in the anomalously large e-ph coupling strength, because the DNL perhaps facilitates new physical effects in the presence of interactions or strong correlations [41]. Here, through first-principles calculations within the framework of DFT [81,82], by employing the QUANTUM ESPRESSO [83] code with the norm-conserving pseudopotential [84] (Supplemental Material [60]), we have revisited the problem of the e-ph coupling strength of the Be (0001) surface by establishing the connection of both the ECF $\alpha^2F(k, \boldsymbol{q}; v)$ and the e-ph coupling strength $\lambda(k, \boldsymbol{q}; v)$ with the DNSSs. Remarkably, we have evidenced the strong e-ph coupling of the DNSSs with the phonon modes, contributing over 80% of the $\lambda^s_{e\text{-ph}}$ of the Be (0001) surface. These results confirm that the anomalously large e-ph coupling strength on the Be (0001) surface is substantially ascribed to the topologically protected DNSSs.

The DNL projection onto the Be (0001) surface forms a closed ring surrounding $\bar{\Gamma}$ in which the DNSSs appear, as discussed in our previously published results [5]. Along the $\bar{K}$-$\bar{\Gamma}$-$\bar{M}$ paths in the surface BZ, these DNSSs [see SF-band1 in Fig. 1(a)] disperse parabolically around the centered $\bar{\Gamma}$ point, in nice agreement with the experimental findings [61,63]. In addition, we have derived the surface phonon dispersions [Figs. 1(b) and 1(d)] in nice agreement with the experimental dispersions [61,62,64,73,74,78] and the previous calculations [75,85]. Particularly, the highly localized surface phonon mode [Rayleigh wave (RW) mode [77]] in Fig. 2(b), dominated by the vibration of the topmost atom along the surface normal, is soft and very sensitive to the interplanar spacing between the first and

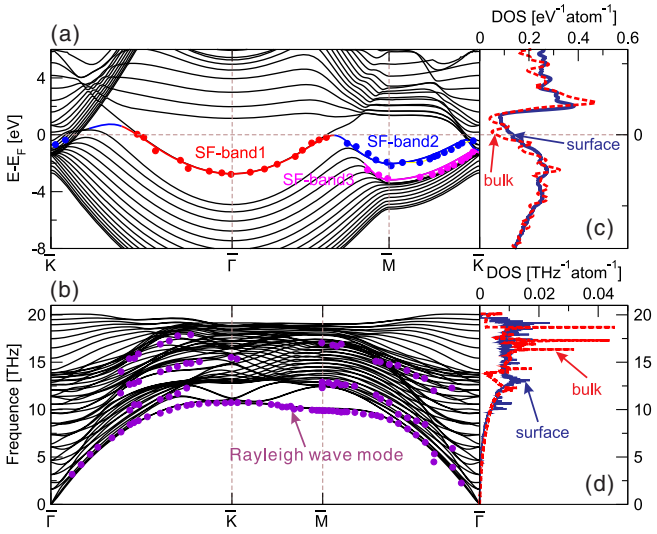

FIG. 1. DFT-derived electronic band structure (a),(c) and phonon dispersion (b),(d) of the Be (0001) surface. (a) The surface electronic structures along the high-symmetric lines as compared with available ARPES experimental data. (b) The surface phonon dispersion along the high-symmetric lines as compared with available experimentally observed surface phonon dispersions. (c),(d) The surface (c) electronic and (d) phononic densities of states (DOSs) in comparison with the total DOSs of its bulk phase.

second topmost atomic layers. In comparison with its bulk phase, the Be (0001) surface shows two apparent differences: (i) the surface electronic DOS at the Fermi level is much larger than that of the bulk phase due to the DNSSs [Fig. 1(c)], and (ii) the two extra peaks at 10 and 11 THz occur in the surface phonon DOS, and the apparent large peak is shifted to a higher frequency of 12.5 THz with respect to that of its bulk phase [Fig. 1(d)].

We have derived the ECF $\alpha^2F(\omega)$ and the e-ph coupling strength λ for both the bulk phase and the (0001) surface. The obtained $\lambda^b_{e\text{-ph}} = 0.254$ for the bulk phase (see Supplemental Material Fig. S2 [60]) and $\lambda^s_{e\text{-ph}} = 0.947$ for the Be (0001) surface [Fig. 2(a)], in nice agreement with the experimental data [0.24 for the bulk phase [71,72], 1.15 ± 0.1 [69] and 1.18 ± 0.07 [70] for the (0001) surface]. The previous calculations [75,80] did not correctly reproduce the frequency ranges of the experimental ECF peaks [78,79] in the low-frequency region along the $\bar{\Gamma}$-$\bar{M}$ direction [Fig. 2(e)]. The conspicuous difference in the ECF was the large peak in the previous calculation [75,80] at about 10 THz, in which the experimental data exhibited a valley [79]. Our current calculations reproduced well these experimentally observed positions of ECF peaks in Fig. 2(e). In order to elucidate whether the electronic DNSSs have effects on the e-ph coupling strength on the Be (0001) surface, we need to derive the ECF $\alpha^2F(\omega)$ at the k momenta where the DNSSs exist in the surface BZ. Hence, we have decomposed the total ECF $\alpha^2F(\omega)$ [86] into the function of each electron momentum (k), each

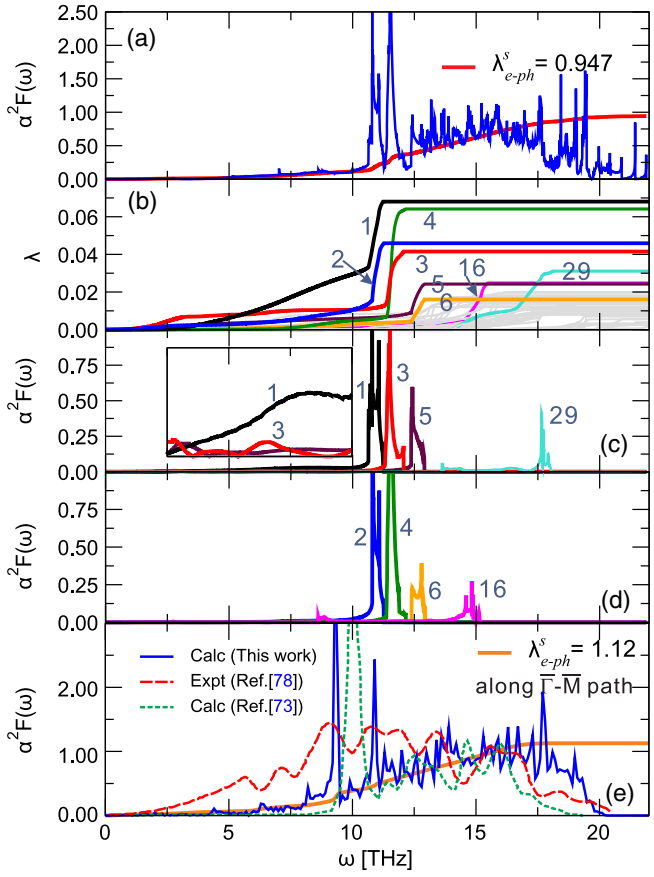

FIG. 2. DFT-derived ECF $\alpha^2F(\omega)$ and the coupling strength λ of the Be (0001) surface. (a) The total ECF and the total e-ph coupling strength. (b) Forty-eight mode-resolved e-ph coupling strengths λ. The λ values of Nos. 1–6, 16, and 29 modes are highlighted, and the other 40 modes are plotted on a gray background. (c),(d) The mode-resolved ECFs for eight selected phonon modes [Nos. 1 (RW mode), 3, 5, and 29 modes in (c). Nos. 2, 4, 6, and 16 modes in (d)]. (e) The derived ECF along the $\bar{\Gamma}$-$\bar{M}$ direction as compared with the ARPES-extracted data multiplied with a factor of 3 for easy comparison [79] and previous calculated data [80].

phonon momentum ($\boldsymbol{q}$), and each phonon mode (v) in the (0001) surface BZ as

$$\alpha^2F(k,\boldsymbol{q};v)=\sum_{i,f}|g_{\boldsymbol{q},v}(k,i,f)|^2\delta(\epsilon_f-\epsilon_i\mp\omega_{\boldsymbol{q},v}),\quad(1)$$

where the term of $g_{\boldsymbol{q},v}(k,i,f)$ is the so-called e-ph matrix element, which represents the probability of electron scattering from an initial electron state i with momentum k to a final electron state f, interacted by a phonon with momentum $\boldsymbol{q}$ and a mode index v. This term can be derived as follows:

$$g_{\boldsymbol{q},v}(k,i,f)=\sqrt{\frac{\hbar}{2M\omega_{\boldsymbol{q},v}}}\langle\varphi_{i,k}|\delta V^{\boldsymbol{q},v}_{\mathrm{scf}}|\varphi_{f,k\pm\boldsymbol{q}}\rangle,\quad(2)$$

where M is the atom mass and $\delta V^{\boldsymbol{q},v}_{\mathrm{scf}}$ is the gradient of the self-consistent potential of the atomic displacements induced by the phonon mode v with momentum $\boldsymbol{q}$ [86]. In addition, the total e-ph coupling strength can be decomposed into $\lambda(\boldsymbol{q};v)$ of each phonon momentum ($\boldsymbol{q}$) and each phonon mode (v) over all electron k momenta in the (0001) surface BZ as

$$\lambda(\boldsymbol{q};v)=2\int\frac{dk}{\Omega_{\mathrm{BZ}}}\frac{\alpha^2F(k,\boldsymbol{q};v)}{N(\epsilon_F)\hbar\omega_{\boldsymbol{q},v}},\quad(3)$$

where $N(\epsilon_F)$ is the electronic DOS at the Fermi level and Ω_{BZ} is the area of the surface BZ. In terms of Eq. (3), we have first calculated mode-resolved λ over all electron k and phonon $\boldsymbol{q}$ momenta in Fig. 2(b) to elucidate the effects of phonon modes on $\lambda^s_{e\text{-ph}}$. It can be seen that the six modes (Nos. 1–6) in the low-frequency region and the two modes (Nos. 16 and 29) in the high-frequency region substantially contribute to the e-ph coupling strength [see Figs. 2(a)–2(c) and Supplemental Material text II [60]]. The No. 1 soft RW mode and No. 2 mode contribute the largest value to λ. Interestingly, we have even recognized that these eight modes exhibit highly localized surface phonon states [Fig. 1(b)].

In order to understand the e-ph coupling between the DNSSs and the ECF (and thus $\lambda^s_{e\text{-ph}}$), we have further derived the $(\boldsymbol{q};v)$-resolved $\lambda(\boldsymbol{q};v)$ values at each phonon vibration $\boldsymbol{v}$ mode and at each phonon $\boldsymbol{q}$ momentum through Eqs. (1) and (3) [see Fig. 3(a), Supplemental Material Tables S1 and S2, and Fig. S3 [60]]. The calculated ECFs [see No. 1 mode in Fig. 3(b)] at the 2D closed circular k momenta around the centered $\bar{\Gamma}$ are anisotropic, and we thus derived $\lambda^s_{e\text{-ph}}$ [Fig. 3(c)] along the directions rotating from $\bar{\Gamma}$-$\bar{M}$ to $\bar{\Gamma}$-$\bar{K}$ (see Supplemental Material Fig. S3 [60]), also evidencing the apparent anisotropy in nice agreement with previous experimental findings [78,79].

Strikingly, the DNSSs exhibit the strong e-ph coupling with the phonon modes. In particular, at the phonon momentum $\boldsymbol{q}=(1/3,1/3,0)$ [87] [Fig. 3(a)], their e-ph couplings are much stronger than those at all the other 34 phonon $\boldsymbol{q}$ momenta (corresponding to six symmetry-inequivalent $\boldsymbol{q}$ momenta in Supplemental Material Table S1 and Fig. S4 [60]). In order to clearly visualize how the DNSSs couple with these vibration modes, we have plotted the mode-resolved ECFs for nine selected vibration modes in the k momenta of the Be (0001) BZ at $\boldsymbol{q}=(1/3,1/3,0)$ [87] in Fig. 3, including the aforementioned eight dominating Nos. 1–6, 16, and 29 modes [Figs. 3(d)–3(k)] and the lowest contributed No. 31 mode [Fig. 3(l)]. For the sake of convenient comparison, the electronic Fermi surface is further plotted in Fig. 3(d) with the aim of showing the exact k momenta where the DNSSs appear. On the one hand, a closed circle surrounding the centered $\bar{\Gamma}$ point exactly corresponds to the DNSSs, as marked by the SF-band1 in Fig. 1(a) and, on the other hand,

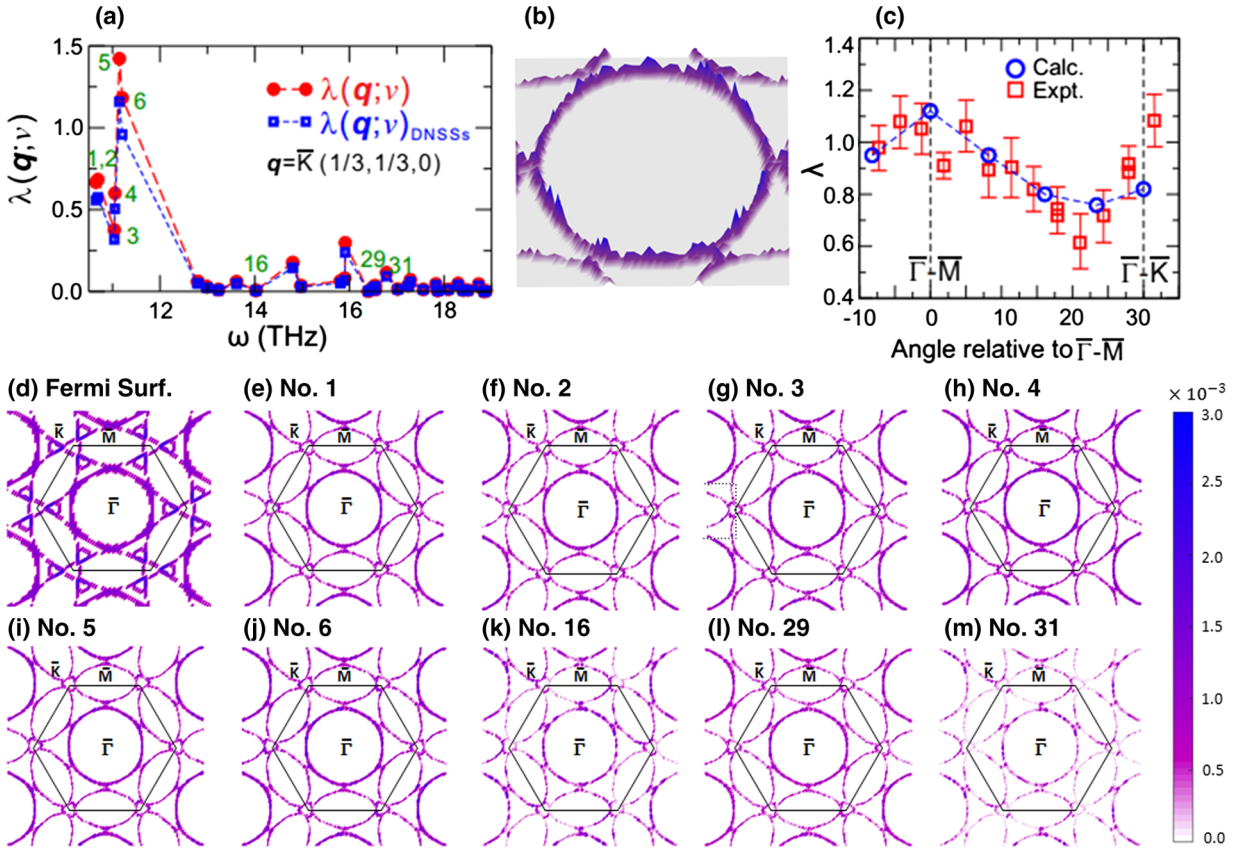

FIG. 3. The $(\boldsymbol{q};\nu)$-resolved λ and ECFs at the phonon $\bar{K}$ momentum $\boldsymbol{q} = (1/3, 1/3, 0)$ [87] on the Be (0001) surface. (a) The $(\boldsymbol{q};\nu)$-resolved λ and the number denotes the corresponding vibration mode (the dashed lines are just a guide to the eye). (b) The 3D plot of the ECF of the No. 1 mode shows a strong anisotropic k-dependent feature. (c) Anisotropic λ along the directions rotating from $\bar{\Gamma}$-$\bar{M}$ to $\bar{\Gamma}$-$\bar{K}$ by varying the angle relative to the $\bar{\Gamma}$-$\bar{M}$ direction. (d) The derived electronic Fermi surface of the Be (0001) surface. (e)–(m) The $(\boldsymbol{q};\nu)$-resolved ECFs of Nos. 1–6, 16, 29, and 31 modes.

three closed trianglelike electronic localized states surrounding the centered $\bar{K}$ point originate from the topologically trivial surface states [5] [SF-band2 and SF-band3 in Fig. 1(a)]. Importantly, for each $\boldsymbol{q}$ momentum exactly on the 2D circular k momenta of the Fermi contour where the DNSSs appear in Fig. 3(d), we have also observed the highest bright closed circular ECFs for all vibration modes, as shown for nine selected modes in Figs. 3(e)–3(m). In contrast, at the trianglelike k momenta around $\bar{K}$, where the trivial surface electronic states appear, the brightness of the ECFs is less weak than that of the centered circular ECFs around $\bar{\Gamma}$. Additionally, it needs to be emphasized that the e-ph couplings are stronger for the eight surface localized phonon modes (Nos. 1–6, 16, and 29 modes) than all other modes. Although the contributions of the other modes to the e-ph coupling are relatively not large, the coupling between the DNSSs and these phonon modes still exist. As evidenced in Fig. 3(m), we have visualized the ECFs of the No. 31 mode that contribute the lowest λ value to $\lambda^{s}_{e\text{-ph}}$; the coupled circular ECF can be clearly observed as well. All these facts clearly evidence the strong couplings of the DNSSs with the phonon vibration modes on the Be (0001) surface, leading to its anomalously large surface e-ph coupling strength.

We have thus calculated the weight of the e-ph coupling between the DNSSs and phonon modes to the total $\lambda^{s}_{e\text{-ph}}$. Through Eq. (3), at each phonon mode and each phonon momentum, we have statistically derived (i) the $\lambda(\boldsymbol{q};\nu)_{\mathrm{DNSSs}}$ associated with the electronic DNSSs by counting the decomposed ECFs over all electronic k momenta on the locations of the DNSSs, (ii) the $\lambda(\boldsymbol{q};\nu)$ over all electron k momenta in the surface BZ, and (iii) their ratio of $w = [\lambda(\boldsymbol{q};\nu)_{\mathrm{DNSSs}}/\lambda(\boldsymbol{q};\nu)]$. Among all the vibration ν modes and the phonon $\boldsymbol{q}$ momenta (see Supplemental Material Tables S1 and S2 [60]), the lowest and highest ratios are $w = 77.6\%$ and $w = 84.5\%$ originating from their e-ph couplings with the No. 45 and No. 3 phonon modes at $\boldsymbol{q} = (1/3, 1/3, 0)$ [87] in Fig. 3(a), respectively. Of course, the surface e-ph coupling strength λ_{DNSSs} over all phonon momenta and all vibration modes can be calculated by counting the ECFs at each k momentum where the DNSSs appear through Supplemental Material

Eqs. (S1) and (S2) [60], consistently revealing that the DNSSs coupled $\lambda^s_{\mathrm{DNSSs}}$ is 80.2% of the total $\lambda^s_{e\text{-ph}}$. Furthermore, we have calculated the $\lambda^s_{e\text{-ph}}$ of the Be (0001) surface by utilizing the electron-phonon Wannier function overlap method [88,89], and a consistent conclusion has been drawn that the DNSSs mainly contribute its surface e-ph coupling enhancement (see Supplemental Material text III and Fig. S5 [60]).

Mechanically, the DNSSs-induced e-ph coupling enhancement is substantially understandable. If we insert the energy factor into Eq. (1) by integrating the electron momenta within the fact that the e-ph coupling mainly occurs at the Fermi level, the ECF can be further expressed as (see Supplemental Material text IV [60])

$$\alpha^2F(\boldsymbol{q};v)=\sum_{k_F,i,f}|g_{\boldsymbol{q},v}(k_F,i,f)|^2N(\epsilon_F), \tag{4}$$

where k_F denotes the electronic momenta where the Fermi surface locates. This equation reveals that the e-ph coupling strength is proportional to $N(\epsilon_F)$, at least in part. The surfaces of the DNL semimetals generally have a very high $N(\epsilon_F)$ due to the presence of the DNSSs and, hence, their surface e-ph coupling enhancements would be reasonably expected. Besides Be, our current calculations at the phononic $\boldsymbol{q}=(0,0,0)$ point of the BZ also evidence the e-ph enhancements of the given surfaces (on which the DNSSs exist) for three other DNL semimetals (C_{24} [6], ZrSiS [16,17] and Cu_3PdN [41,42]) (see Supplemental Material text V and Figs. S6–S8 [60]).

Finally, it is still possible to predict the superconducting T_c of the Be (0001) surface with $\lambda^s_{e\text{-ph}}=0.947$ and $\alpha^2F(\omega)$ using the Dynes modified McMillan formula [90,91]. Its estimated T_c is 15.3–20.5 K using the effective screened Coulomb repulsion constant $\mu=0.10$–0.15. However, even down to 12 K the ARPES experiment revealed no gap of the superconductivity [70]. This superconducting transition still needs to be confirmed, but it would strictly depend on high-quality samples of the Be (0001) surface.

In summary, our Letter demonstrates that the anomalous surface e-ph coupling enhancement of the Be (0001) surface is part of a topological bulk-property correspondence, which highlights potential applications correlated with the e-ph coupling interaction for various topological materials.

This work was supported by the National Science Fund for Distinguished Young Scholars (No. 51725103), by the National Natural Science Foundation of China (Grants No. 51671193 and No. 51474202), and by the Science Challenging Project No. TZ2016004. All calculations were performed on the high-performance computational cluster in the Shenyang National University Science and Technology Park.

*Corresponding author.
xingqiu.chen@imr.ac.cn
†These authors contributed equally to this work.

[1] S. Ryu and Y. Hatsugai, Phys. Rev. Lett. **89**, 077002 (2002).
[2] T. T. Heikkilä and G. E. Volovik, JETP Lett. **93**, 59 (2011).
[3] A. A. Burkov, M. D. Hook, and L. Balents, Phys. Rev. B **84**, 235126 (2011).
[4] H. M. Weng, Y. Y. Liang, Q. N. Xu, R. Yu, Z. Fang, X. Dai, and Y. Kawazoe, Phys. Rev. B **92**, 045108 (2015).
[5] R. Li, H. Ma, X. Cheng, S. Wang, D. Li, Z. Zhang, Y. Li, and X.-Q. Chen, Phys. Rev. Lett. **117**, 096401 (2016).
[6] Z.-Z. Li, J. Chen, S. M. Nie, L. F. Xu, H. Mizuseki, H. M. Weng, and J.-T. Wang, Carbon **133**, 39 (2018).
[7] M. G. Zeng, C. Fang, G. Q. Chang, Y.-A. Chen, T. Hsieh, A. Bansil, H. Lin, and L. Fu, arXiv:1504.3492.
[8] L. Lu, L. Fu, J. D. Joannopoulos, and M. Soljačić, Nat. Photonics **7**, 294 (2013).
[9] K. Mullen, B. Uchoa, and D. T. Glatzhofer, Phys. Rev. Lett. **115**, 026403 (2015).
[10] Y. P. Du, F. Tang, D. Wang, L. Sheng, E.-J. Kan, C.-G. Duan, S. Y. Savrasov, and X. G. Wan, npj Quantum Mater. **2**, 3 (2017).
[11] S.-Y. Yang, H. Yang, E. Derunova, S. S. P. Parkin, B. H. Yan, and M. N. Ali, Adv. Phys. X **3**, 1 (2018).
[12] Q. N. Xu, R. Yu, Z. Fang, X. Dai, and H. M. Weng, Phys. Rev. B **95**, 045136 (2017).
[13] H. Q. Huang, J. P. Liu, D. Vanderbilt, and W. H. Duan, Phys. Rev. B **93**, 201114(R) (2016).
[14] B. J. Feng *et al.*, Nat. Commun. **8**, 1007 (2017).
[15] J.-L. Lu, W. Luo, X.-Y. Li, S.-Q. Yang, J.-X. Cao, X.-G. Gong, and H.-J. Xiang, Chin. Phys. Lett. **34**, 057302 (2017).
[16] L. M. Schoop, M. N. Ali, C. Straßer, A. Topp, A. Varykhalov, D. Marchenko, V. Duppel, S. S. P. Parkin, B. V. Lotsch, and C. R. Ast, Nat. Commun. **7**, 11696 (2016).
[17] J. Hu, Z. Tang, J. Liu, X. Liu, Y. Zhu, D. Graf, K. Myhro, S. Tran, C. N. Lau, J. Wei, and Z. Mao, Phys. Rev. Lett. **117**, 016602 (2016).
[18] C. Fang, H. M. Weng, X. Dai, and Z. Fang, Chin. Phys. B **25**, 117106 (2016).
[19] T. Hyart, R. Ojajärvi, and T. T. Heikkilä, J. Low Temp. Phys. **191**, 35 (2018).
[20] H. Shapourian, Y. X. Wang, and S. Ryu, Phys. Rev. B **97**, 094508 (2018).
[21] N. B. Kopnin, T. T. Heikkilä, and G. E. Volovik, Phys. Rev. B **83**, 220503(R) (2011).
[22] G. E. Volovik, J. Supercond. Novel Magn. **26**, 2887 (2013).
[23] Z. B. Yan, P. W. Huang, and Z. Wang, Phys. Rev. B **93**, 085138 (2016).
[24] W. B. Rui, Y. X. Zhao, and A. P. Schnyder, Phys. Rev. B **97**, 161113(R) (2018).
[25] J. Zhang, M. Gao, J. Zhang, X. Wang, X. Zhang, M. Zhang, W. Niu, and R. Zhang, Front. Phys. **13**, 137201 (2018).
[26] R. Sankar, G. Peramaiyan, I. P. Muthuselvam, C. J. Butler, K. Dimitri, M. Neupane, G. Narsinga Rao, M. T. Lin, and F. C. Chou, Sci. Rep. **7**, 40603 (2017).
[27] M. B. Schilling, L. M. Schoop, B. V. Lotsch, M. Dressel, and A. V. Pronin, Phys. Rev. Lett. **119**, 187401 (2017).
[28] S. P. Mukherjee and J. P. Carbotte, Phys. Rev. B **95**, 214203 (2017).

[29] S. Ahn, E. J. Mele, and H. Min, Phys. Rev. Lett. **119**, 147402 (2017).
[30] J. P. Carbotte, J. Phys. Condens. Matter **29**, 045301 (2017).
[31] S. Pezzini, M. R. van Delft, L. M. Schoop, B. V. Lotsch, A. Carrington, M. I. Katsnelson, N. E. Hussey, and S. Wiedmann, Nat. Phys. **14**, 178 (2018).
[32] L. Gao, J. T. Sun, J. C. Lu, H. Li, K. Qian, S. Zhang, Y. Y. Zhang, T. Qian, H. Ding, X. Lin, S. X. Du, and H. J. Gao, Adv. Mater. **30**, 1707055 (2018).
[33] S. C. Li, Z. P. Guo, D. Z. Fu, X.-C. Pan, J. H. Wang, W. G. Ke, K. J. Ran, S. Bao, Z. Ma, Z. W. Cai, R. Wang, R. Yu, J. Sun, F. Q. Song, and J. S. Wen, Sci. Bull. **63**, 535 (2018).
[34] H. Zhang, Y. Xie, Z. Zhang, C. Zhong, Y. Li, Z. Chen, and Y. P. Chen, J. Phys. Chem. Lett. **8**, 1707 (2017).
[35] M. Hirayama, R. Okugawa, T. Miyake, and S. Murakami, Nat. Commun. **8**, 14022 (2017).
[36] J. X. Li, H. Ma, Q. Xie, S. B. Feng, S. Ullah, R. H. Li, J. H. Dong, D. Z. Li, Y. Y. Li, and X.-Q. Chen, Sci. China Mater. **61**, 23 (2018).
[37] H. M. Weng, Y. Y. Liang, Q. N. Xu, R. Yu, Z. Fang, X. Dai, and Y. Kawazoe, Phys. Rev. B **92**, 045108 (2015).
[38] C. Fang, Y. Chen, H.-Y. Kee, and L. Fu, Phys. Rev. B **92**, 081201(R) (2015).
[39] J. Ahn, D. Kim, Y. Kim, and B.-J. Yang, Phys. Rev. Lett. **121**, 106403 (2018).
[40] Z. J. Wang, B. J. Wieder, J. Li, B. H. Yan, and B. A. Bernevig, arXiv:1806.11116.
[41] Y. Kim, B. J. Wieder, C. L. Kane, and A. M. Rappe, Phys. Rev. Lett. **115**, 036806 (2015).
[42] R. Yu, H. M. Weng, Z. Fang, X. Dai, and X. Hu, Phys. Rev. Lett. **115**, 036807 (2015).
[43] L. S. Xie, L. M. Schoop, E. M. Seibel, Q. D. Gibson, W. W. Xie, and R. J. Cava, APL Mater. **3**, 083602 (2015).
[44] B. J. Wieder and B. A. Bernevig, arXiv:1810.02373.
[45] K. Mullen, B. Uchoa, and D. T. Glatzhofer, Phys. Rev. Lett. **115**, 026403 (2015).
[46] T. Bzdušek, Q. S. Wu, A. Rüegg, M. Sigrist, and A. A. Soluyanov, Nature (London) **538**, 75 (2016).
[47] R. Yu, Q. S. Wu, Z. Fang, and H. M. Weng, Phys. Rev. Lett. **119**, 036401 (2017).
[48] J.-T. Wang, S. M. Nie, H. M. Weng, Y. Kawazoe, and C. F. Chen, Phys. Rev. Lett. **120**, 026402 (2018).
[49] J. X. Li, Q. Xie, S. Ullah, R. H. Li, H. Ma, D. Z. Li, Y. Y. Li, and X.-Q. Chen, Phys. Rev. B **97**, 054305 (2018).
[50] G. Q. Chang, S.-Y. Xu, X. T. Zhou, S.-M. Huang, B. Singh, B. K. Wang, I. Belopolski, J. X. Yin, S. T. Zhang, A. Bansil, H. Lin, and M. Z. Hasan, Phys. Rev. Lett. **119**, 156401 (2017).
[51] R. Bi, Z. B. Yan, L. Lu, and Z. Wang, Phys. Rev. B **96**, 201305(R) (2017).
[52] X. Feng, Q. S. Wu, Y. Cheng, B. Wen, Q. Wang, Y. Kawazoe, and P. Jena, Carbon **127**, 527 (2018).
[53] Y. Sun, Y. Zhang, C.-X. Liu, C. Felser, and B. H. Yan, Phys. Rev. B **95**, 235104 (2017).
[54] Y. Wu, L.-L. Wang, E. Mun, D. D. Johnson, D. X. Mou, L. N. Huang, Y. B. Lee, S. L. Bud'ko, P. C. Canfield, and A. Kaminski, Nat. Phys. **12**, 667 (2016).
[55] G. Bian, T.-R. Chang, H. Zheng, S. Velury, S.-Y. Xu, T. Neupert, C.-K. Chiu, S.-M. Huang, D. S. Sanchez, I. Belopolski, N. Alidoust, P.-J. Chen, G. Q. Chang, A. Bansil, H.-T. Jeng, H. Lin, and M. Z. Hasan, Phys. Rev. B **93**, 121113(R) (2016).
[56] G. Bian *et al.*, Nat. Commun. **7**, 10556 (2016).
[57] M. Neupane, I. Belopolski, M. M. Hosen, D. S. Sanchez, R. Sankar, M. Szlawska, S.-Y. Xu, K. Dimitri, N. Dhakal, P. Maldonado, P. M. Oppeneer, D. Kaczorowski, F. C. Chou, M. Z. Hasan, and T. Durakiewicz, Phys. Rev. B **93**, 201104 (R) (2016).
[58] J.-W. Rhim and Y. B. Kim, Phys. Rev. B **92**, 045126 (2015).
[59] Y. Huh, E.-G. Moon, and Y. B. Kim, Phys. Rev. B **93**, 035138 (2016).
[60] See Supplemental Material at http://link.aps.org/supplemental/10.1103/PhysRevLett.123.136802 which contains (i) details of the computational methods, (ii) Supplementary text I and Fig. S1 of the topological nature of DNL in Be, (iii) DFT *e*-ph coupling calculations (Tables S1 and S2, Figs. S2–S4), (iv) text II of mode-resolved λ over all electron and phonon momenta, (v) text III and Fig. S5 for calculations of electron-phonon coupling using Wannier functions, (vi) text IV of the electron-phonon coupling mechanism from the DNSSs with phonon states, and (vii) text V and Figs. S6–S8 for surface electron-phonon couplings in other DNL semimetals.
[61] E. W. Plummer and J. B. Hannon, Prog. Surf. Sci. **46**, 149 (1994).
[62] U. O. Karlsson, S. A. Flodstrom, R. Engelhardt, W. Gadeke, and E. E. Koch, Solid State Commun. **49**, 711 (1984).
[63] I. Vobornik, J. Fujii, M. Mulazzi, G. Panaccione, M. Hochstrasser, and G. Rossi, Phys. Rev. B **72**, 165424 (2005).
[64] R. A. Bartynski, E. Jensen, T. Gustafsson, and E. W. Plummer, Phys. Rev. B **32**, 1921 (1985).
[65] P. T. Sprunger, L. Petersen, E. W. Pulmmer, E. Laegsgaard, and F. Besenbacher, Science **275**, 1764 (1997).
[66] H. L. Davis, J. B. Hannon, K. B. Ray, and E. W. Plummer, Phys. Rev. Lett. **68**, 2632 (1992).
[67] L. I. Johansson, H. I. P. Johansson, J. N. Andersen, E. Lundgren, and R. Nyholm, Phys. Rev. Lett. **71**, 2453 (1993).
[68] P. J. Feibelman, Phys. Rev. B **46**, 2532 (1992).
[69] T. Balasubramanian, E. Jensen, X. L. Wu, and S. L. Hulbert, Phys. Rev. B **57**, R6866 (1998).
[70] M. Hengsberger, D. Purdie, P. Segovia, M. Garnier, and Y. Baer, Phys. Rev. Lett. **83**, 592 (1999).
[71] G. Grimvall, *The Electron-Phonon Interaction in Metals* (North-Holland, New York, 1981).
[72] G. D. Mahan and E. W. Plummer, in *Electronic Structure*, Handbook of Surface Science Vol. 2, edited by K. Hohn and M. Scheffler (Elsevier, Amsterdan, 2000), Chap. 14, pp. 953–987.
[73] S.-J. Tang, J. Shi, B. Wu, P. T. Sprunger, W. L. Wang, V. Brouet, X. J. Zhou, Z. Hussain, Z.-X. Shen, Z. Zhang, and E. W. Plummer, Phys. Status Solidi B **241**, 2345 (2004).
[74] S. LaShell, E. Jensen, and T. Balasubramanian, Phys. Rev. B **61**, 2371 (2000).
[75] A. Eiguren, S. de Gironcoli, E. V. Chulkov, P. M. Echenique, and E. Tosatti, Phys. Rev. Lett. **91**, 166803 (2003).
[76] J. B. Hannon and E. W. Plumme, J. Electron Spectrosc. Relat. Phenom. **64–65**, 683 (1993).

[77] Ph. Hofmann and E. W. Plummer, Surf. Sci. **377–379**, 330 (1997).
[78] T. Y. Chien, E. D. L. Rienks, M. F. Jensen, P. Hofmann, and E. W. Plummer, Phys. Rev. B **80**, 241416(R) (2009).
[79] T. Y. Chien, X. B. He, S.-K. Mo, M. Hashimoto, Z. Hussain, Z.-X. Shen, and E. W. Plummer, Phys. Rev. B **92**, 075133 (2015).
[80] I. Y. Sklyadneva, E. V. Chulkov, P. M. Echenique, and A. Eiguren, Surf. Sci. **600**, 3792 (2006).
[81] P. Hohenberg and W, Phys. Rev. **136**, B864 (1964).
[82] W. Kohn and L. J. Sham, Phys. Rev. **140**, A1133 (1965).
[83] P. Giannozzi, S. Baroni, N. Bonini, M. Calandra, R. Car, C. Cavazzoni, D. Ceresoli, G. L. Chiarotti, M. Cococcioni, and I. Dabo, J. Phys. Condens. Matter **21**, 395502 (2009).
[84] J. P. Perdew and A. Zunger, Phys. Rev. B **23**, 5048 (1981).
[85] M. Lazzeri and S. D. Gironcoli, Surf. Sci. **402–404**, 715 (1998).
[86] G. Grimvall, in *The Electron-Phonon Interaction in Metals*, Selected Topics in Solid State Physics, edited by E. Wohlfarth (North-Holland, New York, 1981).
[87] For both phonon $\boldsymbol{q}$ and electron $\boldsymbol{k}$ momenta, their units are of reciprocal lattice vectors, unless otherwise explicitly stated.
[88] F. Giustino, M. L. Cohen, and S. G. Louie, Phys. Rev. B **76**, 165108 (2007).
[89] F. Giustino, Jonathan R. Yates, I. Souza, M. L. Cohen, and G. Louie, Phys. Rev. Lett. **98**, 047005 (2007).
[90] W. L. McMillan, Phys. Rev. **167**, 331 (1968).
[91] P. B. Allen and R. C. Dynes, Phys. Rev. B **12**, 905 (1975).